

RESEARCH

Open Access

Modeling and optimization of the line-driver power consumption in xDSL systems

Martin Wolkerstorfer^{1*}, Steffen Trautmann², Tomas Nordström^{1,3} and Bakti D Putra¹

Abstract

Optimization of the power spectrum alleviates the crosstalk noise in digital subscriber lines (DSL) and thereby reduces their power consumption at present. In order to truly assess the DSL system power consumption, this article presents realistic line driver (LD) power consumption models. These are applicable to any DSL system and extend previous models by parameterizing various circuit-level non-idealities. Based on the model of a class-AB LD we analyze the multi-user power spectrum optimization problem and propose novel algorithms for its global or approximate solution. The thereby obtained simulation results support our claim that this problem can be simplified with negligible performance loss by neglecting the LD model. This motivates the usage of established spectral optimization algorithms, which are shown to significantly reduce the LD power consumption compared to static spectrum management.

Keywords: Digital subscriber lines, Energy-efficient, Line driver, Optimization

Introduction

This article analyzes the modeling and optimization of the power consumption in multi-carrier digital subscriber line (DSL) transceivers. The line-driver (LD) power consumption accounts for the largest part in the DSL power budget and scales with the transmit power (TP) [1-3]. With few exceptions [2,4,5], previous study has therefore focussed on minimizing the transmit sum-power [3,6-8] through power spectral optimization, also known as dynamic spectrum management (DSM) [9]. A key feature of this objective is its separability by subcarriers, which is a prerequisite for the Lagrange decomposition [10] of the DSM problem. This decomposition results in low-complexity and even distributed DSM implementations [11-13].

We hypothesize that although TP minimization does not assume knowledge of the underlying LD power consumption, it achieves energy-efficiency at a negligible performance loss compared to a TP optimization taking the LD explicitly into account. In order to support this claim and to realistically assess energy savings by DSM it is indispensable to have an accurate model of the LD power

consumption as a function of the TP. Hence, after providing more background information in Section 'Background information', we begin in Section 'Line driver models' by deriving accurate such models, which are applicable for any DSL technology and different LD classes. While we deem a proof of our hypothesis intractable, we exemplarily provide analytical and numerical evidence supporting our hypothesis based on the proposed enhanced class-AB LD model in Sections 'Optimization models and analysis' and 'Empirical optimization study', respectively. For that purpose we propose two novel numerical approaches for LD power optimization which are based on successive geometric programming (GP) [14,15] and difference-of-convex-functions programming (DCP) [16], respectively. These techniques help us to motivate the selected scenario for simulation of a DSL network with realistic parameters under the two DSM heuristics in [2,3], cf. the introduction in Section 'Empirical optimization study' for a more concise overview of our contributions. The results are rounded off in Section 'Average performance evaluation' by simulations demonstrating the LD power saving potential by energy-efficient multi-user DSM compared to static spectrum management and rate-maximizing DSM. Our conclusions are provided in Section 'Conclusions'.

*Correspondence: wolkerstorfer@ftw.at

¹FTW Telecommunications Research Center Vienna, Donau-City-Straße 1, A-1220 Vienna, Austria

Full list of author information is available at the end of the article

Background information

Energy-efficiency in DSL

In the last ten years, the power consumption of information and communication technology (ICT) has become an issue on top of our agendas, reflecting our concern on global warming, CO₂ emissions and energy sustainability. The telecommunication sector is responsible for 25% of the ICT's energy consumption [17] and therefore energy efficiency has naturally become an issue for industry, standardization, as well as governmental bodies. For example, the share of the fixed broadband access in the telco's energy consumption for 2020 is estimated at around 14% [17]. A related initiative by the European commission aims at a power reduction of 50% in broadband equipment by 2015 [18].

The power consumption of a DSL transceiver can be divided according to its three major parts: the *digital front-end* (the modem's digital signal processing); the *analog front-end* (responsible for the conversion between the analog and the digital domain, including filters); and the *line driver* (the power amplifier driving the line). Depending on the used transmission profile (e.g., bandwidth) the LD power consumption can be somewhere between 30% and 60% of the modem's total power consumption [1-3]. The main focus for energy saving in DSL therefore lies on the LD power consumption [1,4]. Approaches for reducing the power consumption in DSL can be classified into three categories [19]: the optimization of hardware components; dynamic rate adaptation (e.g., by spectral optimization); and low-power modes. Our focus is on the first two approaches, as we a) model the power consumption of an energy-efficient LD type, and b) study energy-efficient DSM based on derived LD power consumption models, leading to lowered transmit rates. We refer to [20,21] for an introduction to LD design for DSL and to [1,22-25] for an overview of various energy saving techniques for DSL.

Line driver modeling

Current DSL systems rely on so called class-AB LDs as these provide a high degree of linearity over a large signal bandwidth. The main drawback of this type of amplifier however lies in its relatively low efficiency. Furthermore, the typical DSL signal exhibits a high crest factor (CF) with high peak values in comparison to its root-mean-square (rms) value. Even though those peak values occur with very low probability, the fixed supply voltage of a Class-AB LD must be sufficiently high to provide distortion-free amplification of the highest signal peaks. This implies that significant power savings could be obtained by modulating the supply voltage to follow the envelope of the amplified signal, as done in so-called class-H LDs. Class-G LDs [20] are class-AB LDs where the supply rail is switched, e.g., between a lower and a higher voltage level V_L and V_H , respectively. The design

of a class-G LD can be differentiated by whether multiple supplies or internal charge pumps are used to provide the multiple supply voltages. In the former design the second supply voltage is typically not directly available on a DSL line card. An additional, costly DC-DC converter is required which must be included in the LD efficiency calculation. A class-H LD can be seen as a class-G LD with an infinite number of supply rails, consequently leading to a higher efficiency at the cost of a more complicated supply design. Altogether we consider the class-G design based on internal charge pumps as the most promising compromise between efficiency and complexity.

As motivated in Section 'Introduction', for the evaluation and optimization of the LD power consumption a realistic functional model is needed which maps the modem's TP to its LD power consumption. An empirical model based on power measurements of a class-AB LD in ADSL2+ was presented in [2]. However, this model is not applicable to other DSL technologies or systems with different physical parameters. A circuit-level model for an LD of class-AB and G with two supplies has been presented in [4], based on the models in [26]. However, these models do not precisely account for the non-idealities of the voltage supply chain [27] (e.g., transformer loss, impedance synthesise factor, etc.) and the power loss in the hybrid circuit. Therefore, in Section 'Class-AB line-driver power model', we derive an enhanced class-AB LD power consumption model based on [26] that can be applied to any DSL profile, and in Section 'Class-G line-driver power model', we propose a novel model for a class-G LD with charge pumps.

Line driver models

Class-AB line-driver power model

In this section, we enhance the functional class-AB LD model in [26] based on a circuit analysis, cf. Figure 1. The total power consumed by a class-AB LD is given as

$$P_{LD(AB)} = P_u + P_{diss} + P_{Hybrid}, \quad (1)$$

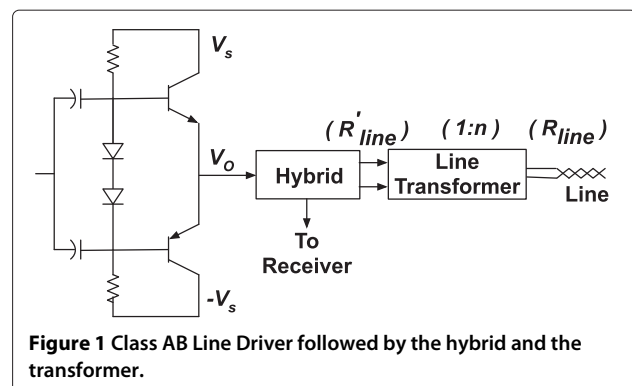


Figure 1 Class AB Line Driver followed by the hybrid and the transformer.

where P_u is the output power measured at the LD output of a line indexed by $u \in \mathcal{U}$, P_{diss} is the total power dissipated inside the LD, and P_{Hybrid} is the power consumed by the hybrid circuit. The level of P_{Hybrid} strongly depends on the hybrid implementation and topology and ranges from a few mW to several tens of mW. By the reformulation detailed in Appendix 1 the LD power consumption in (1) can be equivalently written as

$$P_{\text{LD(AB)}} = V_s \cdot \left(I_Q + \sqrt{\frac{2}{\pi} \frac{P_u}{R'_{\text{line}}}} \right) + P_{\text{Hybrid}}, \quad (2)$$

where V_s is the supply voltage of the LD, I_Q is the quiescent current, and R'_{line} as defined in Appendix 1 is the transformed resistance of the line, cf. Figure 1. In the ideal case the supply voltage V_s can be designed to cover the output voltage swing $CF \cdot V_{\text{rms,ideal}}$ described by the signal crest factor CF and the ideal rms LD output voltage $V_{\text{rms,ideal}}$ [26].

However, a more realistic representation of V_s should include several impairments that will generally be present in real implementations and significantly influence the LD efficiency:

- 1) The achievable signal swing at the LD output is reduced from its theoretical maximum value V_s by a voltage drop V_{drop} . Its value is typically in the range between 2 and 4 V, and determined by the design and the underlying technology of the LD output stage.
- 2) The resistances of the copper coils and other non-idealities cause an additional voltage drop over the transformer. This loss in effective signal power on the line is called transformer loss TL and can reach 0.2 to 0.5 dB for EP5 and EP7 transformers as used in xDSL central office (CO) applications.
- 3) Another voltage drop occurs in the termination circuitry. Impedance synthesis is a commonly used concept in LD system integration [28] to reduce this

loss. More precisely, only a small part of the effective receive signal termination is provided by an external resistor, while the main part is actively generated by the LD itself. The impedance synthesis factor m - that is the ratio between the external resistor value and the over-all termination resistance - also determines the receive signal attenuation and cannot be made arbitrarily small. Therefore, a voltage drop by a factor $m/(m+1)$ must be included in the calculation of the required LD supply voltage. While for VDSL2 systems a reasonable choice of m lies in the range from 3 to 6, for pure ADSL/ADSL2+ systems a more aggressive choice of m in the range from 6 to 20 is possible.

Using $V_{\text{rms,ideal}} = \sqrt{P_u \cdot R'_{\text{line}}}$ these additional factors can be accommodated in the form

$$V_s = CF \cdot \sqrt{\hat{P}_u \cdot R'_{\text{line}}} \cdot \text{TL} \cdot \frac{m+1}{m} + V_{\text{Drop}}, \quad (3)$$

where \hat{P}_u is the maximum transmitted power. Figure 2 depicts an exemplary measurement of a real ADSL2+ LD's power consumption, as well as the class-AB LD power consumption model^a in (2), using (a) the mentioned ideal relation $V_s = CF \cdot V_{\text{rms,ideal}}$, (b) the relation $V_s = CF \cdot V_{\text{rms,ideal}} + V_{\text{drop}}$ with headroom V_{drop} as used in [4], and (c) the relation derived in (3). From this plot it is visible that there is a considerable amount of LD power consumption that has not been taken into account by previous models.

Based on the wide deployment of class-AB LDs and the simple functional shape of our model we will focus on this LD type when analyzing the effect of the LD on energy-efficient DSM in Sections 'Optimization models and analysis', 'Empirical optimization study', and 'Average performance evaluation'. Another energy-saving approach mentioned in Section 'Energy-efficiency in DSL' is the

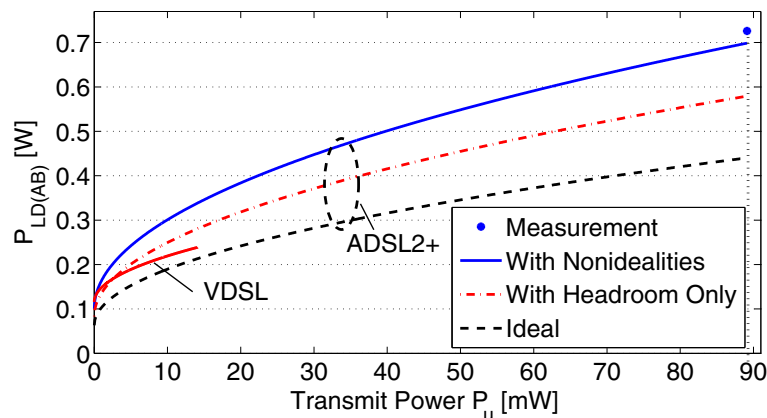


Figure 2 Comparison of class-AB LD power models. The figure shows the influence of additional non-idealities considered in our LD model.

deployment of more energy-efficient LDs, as analyzed in the following section.

Class-G line-driver power model

Based on our discussion in Section ‘Line driver modeling’, we study in this section class-G LDs with a set of internal charge pumps. We refer to Appendix 2 for a model of an LD with two supply voltages that includes the non-idealities discussed in Section ‘Class-AB line-driver power model’ into the model in [4,26]. The basic principle of a charge pump is exemplified in Figure 3. A pair of such charge pumps is used to generate the high class-G supply voltage V_H from a single LD supply voltage which at the same time serves as the low class-G supply voltage V_L . Under ideal conditions, a maximum voltage ratio of $V_H/V_L = 3$ can be achieved. However, taking technological limitations and various internal voltage drops into account, assuming a ratio of $V_H/V_L \approx 2$ is more realistic. The total power consumption of a class-G LD with internal charge pumps is defined as

$$P_{LD(G-CP)} = P_{Low,CP} + P_{High,CP} + P_{Q,CP} + P_{Hybrid}, \quad (4)$$

where $P_{Low,CP}$ is the LD power consumption value of an equivalent class-AB LD running continuously at the low voltage supply, and $P_{High,CP}$ refers to the additional power consumption when the LD is switching to the high voltage supply. $P_{Q,CP}$ is the quiescent power dissipation. The voltage level V_H is thought of as the summation of V_L and $V_H - V_L$, with the latter being generated by the charge pumps when needed. The consumed LD power at the low voltage V_L is in analogy to (2) defined as

$$P_{Low,CP} = V_L \cdot \sqrt{\frac{2}{\pi} \frac{P_u}{R'_{line}}}. \quad (5)$$

Extending the ideal rms voltage $V_{rms,ideal} = \sqrt{P_u \cdot R'_{line}}$ with the non-idealities of Section ‘Class-AB line-driver

power model’ we obtain the rms LD output voltage (that is, before impedance synthesis and transformer) as

$$V_{rms} = \sqrt{P_u R'_{line}} \cdot TL \cdot \frac{m+1}{m}. \quad (6)$$

In analogy to the ideal class-G case [26] the mean average deviation (MAD) of the LD output voltage for the cases when the Gaussian distributed output signal is below and above the threshold $V_{th} = (V_L - V_{drop})$ is given as

$$V_{MAD,Low} = \sqrt{\frac{2}{\pi}} V_{rms} \left(1 - e^{-\frac{V_{th}^2}{2V_{rms}^2}} \right), \quad (7)$$

and

$$V_{MAD,High} = \sqrt{\frac{2}{\pi}} V_{rms} e^{-\frac{V_{th}^2}{2V_{rms}^2}}, \quad (8)$$

respectively. Note that the fraction of time $\mu_{cp}(P_u) \in [0, 1]$ the charge pump is used is higher than the time the output signal exceeds the threshold V_{th} , the reason being the additional ramp-up / ramp-down phases between the low and the high supply. Therefore the output signal’s MAD during charge pump usage is a combination of that when the signal is below and above V_{th} , respectively, weighted by the corresponding probabilities. The output signal’s MAD under the assumption of operating below and above the threshold is given by $V_{MAD,Low}/(1 - 2Q(\frac{V_{th}}{V_{rms}}))$ and $V_{MAD,High}/(2Q(\frac{V_{th}}{V_{rms}}))$, respectively. Correspondingly we define the dynamic power $P_{High,CP}$ as

$$P_{High,CP} = \frac{V_H - V_L}{R'_{line} TL \frac{m+1}{m}} (\mu_A \cdot V_{MAD,Low} + \mu_B \cdot V_{MAD,High}) \cdot \rho, \quad (9)$$

where

$$\mu_A = \frac{\mu_{cp}(P_u) - 2Q(\frac{V_{th}}{V_{rms}})}{1 - 2Q(\frac{V_{th}}{V_{rms}})}, \quad (10)$$

$\mu_B = 1$, $Q(\cdot)$ is the Q-function, ρ is the recharge loss, and the term $R'_{line} TL \frac{m+1}{m}$ represents the total resistance at the LD output. Comparing the total dynamic power (the sum of (5) and (9)) to that under a class-G design with two supplies (the sum of (30a) and (31) in Appendix 2) we find that the latter one is obtained by setting $\mu_A = 0$ and $\rho = 1$. We emphasize that $\mu_{cp}(P_u)$ depends not only on the output power, but, for example, also on the transformer ratio, the DSL profile, or the way in which the charge pump is loaded. The quiescent power consists, differently to that in class-AB LDs, of three main components, given as

$$P_{Q,CP} = P_{Q,Low} + P_{Q,High} + P_{Q,class-G}. \quad (11)$$

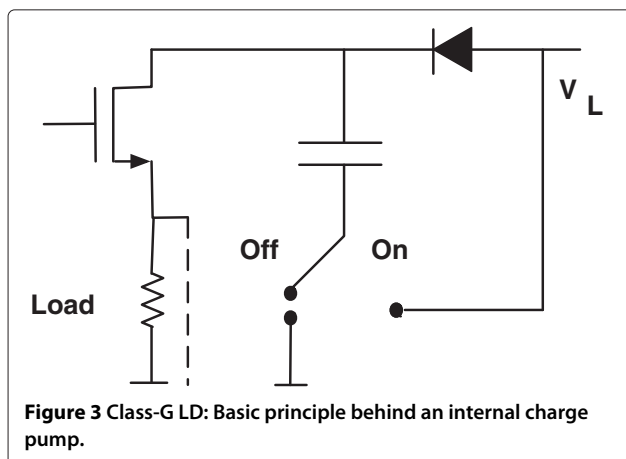


Figure 3 Class-G LD: Basic principle behind an internal charge pump.

The term $P_{Q,Low} = V_L \cdot I_Q$ is the quiescent power dissipation of an equivalent class-AB LD continuously working at V_L . The additional quiescent power dissipation of the LD when working at the high voltage supply is defined as

$$P_{Q,High} = (V_H - V_L) \cdot I_Q \cdot \mu_{cp}(P_u) \cdot \rho. \quad (12)$$

The third term in (11) splits into

$$P_{Q,classG} = (V_L + (V_H - V_L) \cdot \mu_{cp}(P_u) \cdot \rho) \cdot I_{Q,classG} + L_{classG}, \quad (13)$$

where $I_{Q,classG}$ is the additional quiescent current in class-G mode and L_{classG} [W] refers to further fixed losses in the class-G circuitry.

In Figure 4, we compare the power consumption data provided for a real class-G LD with charge pumps in [29] to the three discussed LD models: our model of a class-G LD with charge pumps in this section, the model of a class-G LD with two power supplies in Appendix 2, and the model of a class-AB LD modeled by Equations (2) and (3), respectively^b. In Figure 4a we see that under an ADSL2+ profile the power consumption predicted by our model of a class-G LD with charge pumps lies between that calcu-

lated by the models of a class-AB LD and a class-G LD with two supplies. Figure 4b shows that the class-G LD models lead to similar power estimates for transmit powers below 14.5dBm. This is explicable by the fact that a low transmit power leads to low probabilities $\mu_{cp}(P_u)$ and $\mu_{2S}(P_u)$ of using the high supply in the class-G LD with charge pumps and with two supplies (see Appendix 2), respectively. Correspondingly we can approximate the power consumption of a class-G LD for low transmit power values by that of a class-AB LD in (5) that operates at the low supply voltage. However, near the maximum output power the novel class-G LD model with charge pumps significantly deviates from the class-G LD model with two supplies, similarly as the consumption of the real LD described in [29]. For example, at the maximum transmit power of 20.5dBm the two-supply class-G LD model underestimates the power consumption of the LD in [29] by as much as 44mW for ADSL2+ or 83mW for VDSL2 8b. Regarding for instance the curves for VDSL2 30a we find that the real consumption values are partially below the class-G LD models for higher transmit powers. This can be explained by the deviation of the quiescent current into the load [28] which is circuit and transmit power dependent. Differently, all the presented LD models (as well as those in [4,26]) assume a constant quiescent current I_Q that is independent of the transmit power.

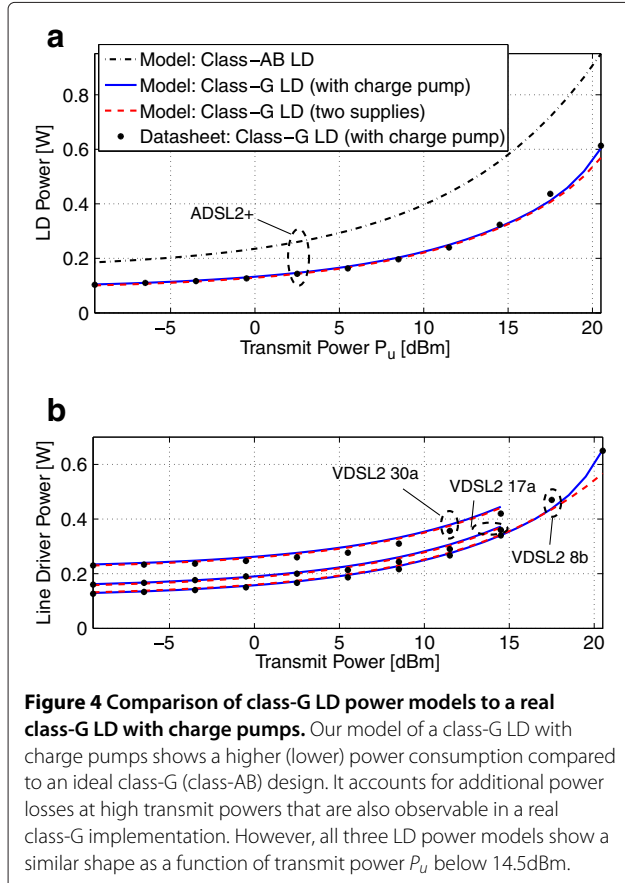
In summary, the class-G design with charge pumps yields substantial energy savings compared to a class-AB LD while sparing us the DC-DC conversion needed for class-G LDs with two supplies. Furthermore, the presented LD power models have a qualitatively similar functional shape for transmit power values below 14.5dBm as they are all based on the elementary class-AB power relation in (2). In the following sections, we focus on the class-AB LD and analyze our hypothesis of Section 'Introduction' on the difference between LD power and TP optimization.

Optimization models and analysis

In this section, we want to formally develop some insight into *when* a difference between LD power and TP optimization in terms of the achieved class-AB LD power might occur, how large it is, and whether this difference truly occurs under realistic network conditions.

DSL system model and notation

Current DSL systems employ frequency-division duplexing (FDD) and discrete multi-tone (DMT) modulation which splits the available frequency bandwidth into C orthogonal subchannels (subcarriers). Our system model consists of U subscriber lines sharing a single cable binder. Electromagnetic coupling between the users' twisted pair wires leads to crosstalk noise at the receivers, which is the reason for performing the power allocation



of all users jointly. The achievable rate per DMT-symbol $r_c^u(\mathbf{p}_c)$ for user $u \in \mathcal{U} = \{1, \dots, U\}$ on subcarrier $c \in \mathcal{C} = \{1, \dots, C\}$ as a function of the signal to interference and noise ratio (SINR) is modeled by the common gap-approximation [30]

$$r_c^u(\mathbf{p}_c) = \log_2 \left(1 + \frac{H_c^{uu} p_c^u}{\Gamma \left(\sum_{i \in \mathcal{U} \setminus u} H_c^{ui} p_c^i + N_c^u \right)} \right), \quad (14)$$

where $\mathbf{p}_c = [p_c^1, \dots, p_c^U]^T$, p_c^u is the power assigned to subcarrier c of user u , and the terms H_c^{uu} and H_c^{ui} are the direct channel transfer coefficient of user u and the cross-channel transfer coefficient from user i to user u on subcarrier c , respectively. DSM implementations in standard-compliant DSL systems, including crosstalk estimation functionality, have been reported in [31,32]. The term Γ indicates the SNR-gap to capacity depending on the modulation scheme, the targeted bit-error rate, the coding gain, and the noise margins, while N_c^u represents the total received background noise power on subcarrier c of user u , including white thermal noise, alien-crosstalk, and radio-frequency interference.

Based on Section ‘Line driver models’, the LD power consumption of a class-AB LD as a function of the total TP $P_u = \sum_{c \in \mathcal{C}} p_c^u$ of user u is given in the form

$$f_u^{\text{LD}}(P_u) = \hat{w}_u \sqrt{P_u} + \check{w}_u, \quad (15)$$

where the parameters $\hat{w}_u \in \mathcal{R}_+$ and $\check{w}_u \in \mathcal{R}_+$ are dependent on the hardware and system model^c. In the following optimization study, we will use two key features of this function: a) it is monotonously increasing, and b) concave in P_u (or p_c^u , $c \in \mathcal{C}$, respectively).

Optimization problems

Similarly as in previous DSL studies [11,33] we mathematically formulate the problem of minimizing the transmit sum-power in DSL in the form

$$J^{\text{TP}} = \underset{p_c^u, u \in \mathcal{U}, c \in \mathcal{C}}{\text{minimize}} \sum_{u \in \mathcal{U}} \sum_{c \in \mathcal{C}} p_c^u \quad (16a)$$

$$\text{subject to } \sum_{c \in \mathcal{C}} r_c^u(\mathbf{p}_c) \geq R_u, \quad \forall u \in \mathcal{U}, \quad (16b)$$

$$\sum_{c \in \mathcal{C}} p_c^u \leq \hat{P}_u, \quad \forall u \in \mathcal{U}, \quad (16c)$$

$$0 \leq p_c^u \leq \hat{p}_c^u, \quad \forall c \in \mathcal{C}, \forall u \in \mathcal{U}, \quad (16d)$$

$$r_c^u(\mathbf{p}_c) \leq \hat{B}, \quad \forall c \in \mathcal{C}, \forall u \in \mathcal{U}, \quad (16e)$$

where $\hat{p}_c^u, c \in \mathcal{C}, u \in \mathcal{U}$, denotes the PSD mask, \hat{B} the maximum number of bits that can be allocated to a single subcarrier, and R_u and \hat{P}_u the target-rate per DMT-symbol and the maximum sum-power of user u , respectively. In practice numerous other objectives may be targeted besides energy consumption, including for example sum-rate [33], fairness [34], service coverage [35], the energy-per-bit [8], or weighted combinations thereof [6]. However, our choice of focusing on energy-minimization subject to rate-constraints will allow us to study various defined rate combinations. Similarly to (16), based on the model in (15) the problem of minimizing the total LD power consumption in DSL can be stated as

$$J^{\text{LD}} = \underset{p_c^u, u \in \mathcal{U}, c \in \mathcal{C}}{\text{minimize}} \sum_{u \in \mathcal{U}} \sqrt{\sum_{c \in \mathcal{C}} p_c^u} \quad (17a)$$

$$\text{subject to Constraints (16b)–(16e),} \quad (17b)$$

where for simplicity of exposition we assume identical LD models for all users. This allows us to omit the added constant \check{w}_u and the factor \hat{w}_u , $u \in \mathcal{U}$, as they have no influence on the optimal solution. Note that the latter factors can easily be reintroduced under the numerical optimization approaches in Section ‘Empirical optimization study’. For instance, heterogeneous LD models are considered for the simulations in Section ‘An experiment in real-sized DSM problems using heuristics’. For brevity we will denote the optimal per-user sum-power values for the problems in (16) and (17) by $\mathbf{P}^{\text{TP}} \in \mathcal{R}_+^U$ and $\mathbf{P}^{\text{LD}} \in \mathcal{R}_+^U$, respectively.

Analysis of the optimization problems in (16) and (17)

Before turning to the numerical optimization of the problems in (16) and (17) we analyze their solutions and the difference between their solutions in terms of LD power independently of their exact solution value. To begin with we define the set of possible solutions (the ‘power-region’).

Definition 1 (Power-region). *The power-region associated with the problems in (16) and (17) is defined as the set*

$$\mathcal{P} = \{ \mathbf{P} \in \mathcal{R}_+^U \mid \exists p_c^u, c \in \mathcal{C}, u \in \mathcal{U}, \text{feasible for constraints (16b)–(16e), } P_u = \sum_{c \in \mathcal{C}} p_c^u \}. \quad (18)$$

Proposition 1. *The sum-power vectors \mathbf{P}^{TP} and \mathbf{P}^{LD} achieved at a solution of the power minimization problems in (16) and (17), respectively, both lie on the boundary of*

the power-region \mathcal{P} as defined in (18), i.e., $\nexists \mathbf{P} \in \mathcal{P}, \mathbf{P} \neq \mathbf{P}^{\text{TP}}, \mathbf{P} \preceq \mathbf{P}^{\text{TP}}$ and $\nexists \mathbf{P} \in \mathcal{P}, \mathbf{P} \neq \mathbf{P}^{\text{LD}}, \mathbf{P} \preceq \mathbf{P}^{\text{LD}}$.

Proof. The proof simply follows from the monotonicity of the objectives in (16a) and (17a), respectively. \square

Proposition 1 also suggests a practical heuristic approach for LD power optimization, namely through a sequence of weighted sum-power minimizations with weights based on the projected gradients of the objective functions $f_u^{\text{LD}}(P_u)$, cf. [36] where a similar idea was applied for a rate-utility maximization problem. However, while in [36] a non-concave maximization was performed over the rate-region, here we face a concave *minimization* problem over the power-region.

The following proposition identifies the smallest problem instances where a difference between the two problems in terms of LD power may occur, and which we will further study in Section ‘Empirical optimization study’.

Proposition 2. *Differences between the optimal solutions of the problems in (16) and (17) in terms of LD power can only occur for $U \geq 2$ and $C \geq 2$.*

See Appendix 3 for a proof.

Next, we define the relative gain by LD power optimization in (17) compared to TP minimization in (16) as

$$\xi = \frac{\hat{w} \sum_{u \in \mathcal{U}} \left(\sqrt{P_u^{\text{TP}}} - \sqrt{P_u^{\text{LD}}} \right)}{\hat{w} \sum_{u \in \mathcal{U}} \sqrt{P_u^{\text{TP}}} + U \cdot \check{w}}, \quad (19)$$

where in the nominator we have the difference in LD power between the two optimization approaches we are interested in, and in the denominator the LD power under the TP minimization. In other words, the relative gain in (19) tells us how much more energy-efficient LD power optimization is compared to classical TP minimization. In the following we derive a bound on ξ for any number of users U and subcarriers C with powers p_c^u summing to the total power $P_u = \sum_{c \in C} p_c^u$. More precisely, we have

$$\sqrt{\sum_{u \in \mathcal{U}} P_u^{\text{TP}}} \leq J^{\text{LD}} \leq \sum_{u \in \mathcal{U}} \sqrt{P_u^{\text{TP}}}, \quad (20)$$

where the first inequality holds due to the monotonicity and concavity of the model in (15), and the optimality of $\sum_{u \in \mathcal{U}} P_u^{\text{TP}}$ in (16), and the second inequality holds due to feasibility of a solution to the problem in (16) for the problem in (17). Using (20) in (19) we obtain the bound

$$\xi \leq \frac{\hat{w} \left(\sum_{u \in \mathcal{U}} \sqrt{P_u^{\text{TP}}} - \sqrt{\sum_{u \in \mathcal{U}} P_u^{\text{TP}}} \right)}{\hat{w} \sum_{u \in \mathcal{U}} \sqrt{P_u^{\text{TP}}} + U \cdot \check{w}}, \quad (21)$$

which is only dependent on the solution of the problem in (16) and illustrated in Figure 5. Expanding our intuition from Proposition 2, we see that this simple bound does not allow for any LD power reduction by direct LD power optimization in (17) compared to TP minimization in (16) when all but one user transmit with very low power (e.g., below -20 dBm). Note however that Figure 5 does not allow us to make any conclusions on possible differences when all lines operate in a high-power regime. For example, if the solution to the TP minimization problem in (16) demands all users to use maximum sum-power, by sum-power optimality in (16) the same must hold in the LD power minimization problem in (17) and so the difference between the two must actually vanish, differently to what the bound in (21) indicates. Using Jensen’s inequality we can even bound (21) independently of the solution \mathbf{P}^{TP} , giving

$$\xi \leq \left(1 - \frac{1}{\sqrt{U}} \right) \left(1 + \frac{\check{w} \sqrt{U}}{\hat{w} \sqrt{\sum_{u \in \mathcal{U}} \hat{P}_u}} \right)^{-1}. \quad (22)$$

The gain ξ for $U = 2$ users is for instance bounded by $1 - 1/\sqrt{U}$ ($\approx 30\%$). The bounds in (21) and (22) are identical when $P_u^{\text{TP}} = \hat{P}_u = P, \forall u \in \mathcal{U}$.

In this section, we have located the solutions of our two optimization problems on the boundary of a power-region and identified potentially insightful problem instances. In the following section, we will use this information to study the real gain ξ by directly optimizing the LD power model through numerical methods.

Empirical optimization study

We will use three approaches to obtain insights into the differences between TP and LD power minimization in terms of the LD power consumption founded on the functional model in (15): The first one is based on an efficient but possibly suboptimal successive geometric

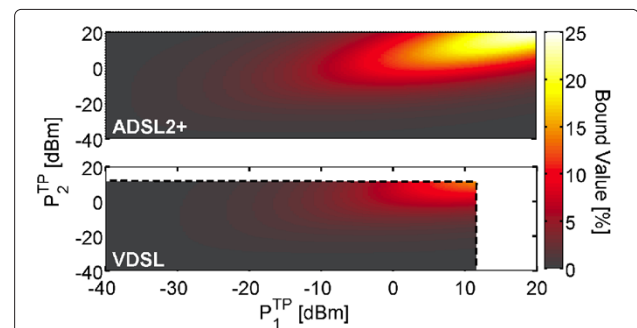


Figure 5 Bound on the LD power difference between two optimization objectives. Upper-Bound in (21) on the LD power difference between the solutions of the problems in (16) and (17) for $U = 2$ users.

programming (GP) approximation used in order to identify problem parameters under which differences between the optimal solutions of the two optimization problems occur. While it is known [15] that the TP optimization problem can be approached by GP, our contribution is to recognize this fact for the LD power optimization problem. The second approach is based on the globally optimal solution of both problems in (16) and (17). Global optimality is a necessary property to study the power-region in Definition 1 and the location of the solutions to the problems in (16) and (17) in this region. Furthermore, it allows us to provide an exemplary scenario where provably a difference between the solutions of the two optimization problems occurs. For solving these non-convex and rate-constrained LD power and TP optimization problems we found it necessary to develop a problem-specific algorithm. It deviates in various aspects from the approaches proposed for related rate-maximization problems in [37,38], e.g., it allows for an optimization over all subcarriers including a non-convex constraint set, and uses improved branching and bounding techniques. The third approach is by the heuristic successive convex approximation algorithms proposed in [2,11], respectively. These two algorithms allow to study problem instances of realistic size and channel parameters.

DSM based on successive SINR-approximation and geometric programming

Geometric programs (GP) are a class of problems which is not convex but can easily be converted into a convex form by logarithmic transformations [14]. This optimization model was applied to power control in [15,39], where also successive GP approximations were proposed for non-convex problems based on monomial [14] or SINR approximations [11]. For a short introduction to GP and the corresponding problem transformation of the LD power optimization problem in (17) we refer to Appendix 4.

As mentioned above our motivation for applying successive GP is to solve numerous small problem instances ($U = C = 2$) in order to identify problem parameters which lead to a substantial gain ξ by LD power optimization compared to TP optimization. We generated numerous problem instances of (16) and (17) by setting H_c^{21} and H_c^{12} to all combinations out of the set $\{-90, -67.5, -45, -22.5, 0\}$ dB, and for each of these combinations forming all target-rate combinations sampling the users' possible rates at 20 equi-distant rate-levels from 0 to the maximum achievable rate (i.e., 400 rate-combinations)^d. After running successive GP for the problems in (16) and (17) we re-initialize the algorithm with the obtained result for the respective other problem and keep the best solution found for each problem^e. Also, we multiply the per-user sum-powers by a factor of 500

before applying the LD power model in order to obtain a more realistic estimate of the LD power savings^f. The result of this experiment can be summarized as follows: Significant values of ξ occurred under unsymmetric settings of target-rates and crosstalk coefficients, especially so when the stronger disturber is the one having the larger target-rate, cf. Figure 6. Intuitively this kind of setup results in one user operating with low sum-power (where the derivative of the LD power model in (15) is high) while the user with the larger target-rate operates with higher sum-power (corresponding to a lower derivative of the LD power model in (15)). From a sum-power perspective it may make sense to allow the strong disturber to interfere with the weak disturber due to his higher target-rates. However, from an LD power perspective the user with the low target-rates is worth protecting more due to the larger derivative of the LD power model at low sum-power values, cf. the LD power model in Figure 2.

In the following section, we select a specific scenario based on these insights for further investigation.

Global solutions of non-convex LD power optimization problems using difference-of-convex-functions programming (DCP)

Difference-of-convex-functions programming (DCP) [40] is a widely applicable approach in global optimization where non-convex objective and constraint functions are reformulated as the difference of convex functions, cf. [37,38] for recent applications in power control. Similarly to the reformulation shown in [37,38] for a rate-maximization problem, the rate-constraints in (16b) can be equivalently written as

$$-\sum_{c \in C} r_u^c(\mathbf{p}^c) + R_u = g_u(\mathbf{p}) - h_u(\mathbf{p}) \leq 0, u \in U, \quad (23)$$

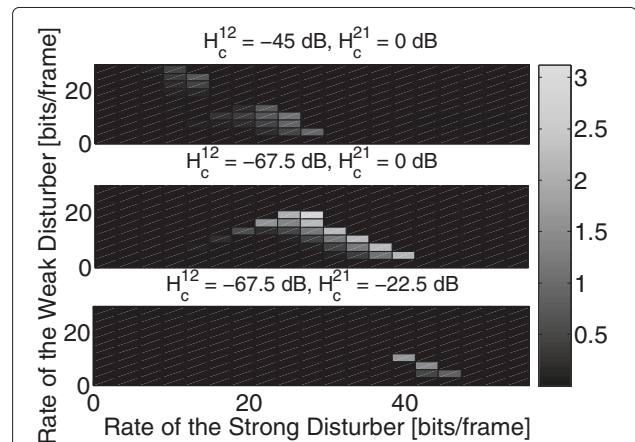


Figure 6 Gain by direct LD power optimization. Percent gain ξ by direct LD power optimization compared to TP optimization obtained through the suboptimal successive GP algorithm.

where

$$g_u(\mathbf{p}) = -\sum_{c \in \mathcal{C}} \log \left(H_{uu}^c p_u^c + \sum_{j \in \mathcal{U} \setminus \{u\}} \Gamma H_{uj}^c p_j^c + \Gamma N_u^c \right) + R_u, \quad (24)$$

$$h_u(\mathbf{p}) = -\sum_{c \in \mathcal{C}} \log \left(\sum_{j \in \mathcal{U} \setminus \{u\}} \Gamma H_{uj}^c p_j^c + \Gamma N_u^c \right), \quad u \in \mathcal{U}, \quad (25)$$

are convex functions. Writing the objective in (17a) formally as $0 - h_0(\mathbf{p})$ with convex function $h_0(\mathbf{p}) = -\sum_{u \in \mathcal{U}} \sqrt{\sum_{c \in \mathcal{C}} p_c^u}$ we can write the problem in (17) as the following DCP problem [40],

$$\text{minimize } -h_0(\mathbf{p}) \quad (26a)$$

$$\text{subject to } g_u(\mathbf{p}) - h_u(\mathbf{p}) \leq 0, \quad u \in \mathcal{U} \quad (26b)$$

$$\text{Constraints (16c)–(16e)}. \quad (26c)$$

While in previous applications of DCP in the area of power control [37,38] the problem was in fact solved as a concave minimization problem over a convex constraint set, we have additionally complicating DCP constraints in (26b). Correspondingly we developed a more general solution approach, namely a box-based branch-and-reduce algorithm initialized by a successive GP [15] solution, cf. Appendix 5 for details. Note that this DCP algorithm can similarly be applied to (optimally) solve the TP problem in (16).

We use the developed global optimal algorithm to investigate the power-region as given in Definition 1. For reasons of tractability we restrict ourselves to a specific scenario ($U = C = 2$) identified using the heuristic in Section ‘DSM based on successive SINR-approximation

and geometric programming⁸. In Figure 7, we show the power-regions and the solutions of the problems in (16) and (17) for varying crosstalk parameter H_c^{21} . First, we see that both solutions \mathbf{P}^{TP} and \mathbf{P}^{LD} lie on the power-region, as predicted by Proposition 1. However, the solutions lie on different contour lines of the function $\sum_{u \in \mathcal{U}} \sqrt{P_u}$, meaning that they provably differ in terms of LD power consumption. While the TP solution minimizes $[0.5, 0.5] \cdot \mathbf{P}$ over the power-region, the LD power optimal solution minimizes $[0.17, 0.83] \cdot \mathbf{P}$. In other words, the LD power optimum is attainable by a weighted sum-power optimization with specific weights. Searching for these weights is in fact the idea behind the projected gradient heuristic indicated in Section ‘Analysis of the optimization problems in (16) and (17)’. With a decreasing parameter H_1^{21} the needed sum-powers for constant target-rates decrease, leading to a decrease of the achievable gain ξ by LD power optimization compared to TP minimization, cf. Figure 7.

An experiment in real-sized DSM problems using heuristics

In this section, we compare solutions obtained by two DSM heuristics and static spectrum management (SSM) in terms of their LD power: (a) the successive convex approximation algorithm [3] for the problem in (16) which is based on the convex approximation $\tilde{r}_c^u(\mathbf{p}_c)$ of the rate-function $r_c^u(\mathbf{p}_c)$ as given in Appendix 4 and introduced in [11] for a rate-maximization problem in DSL; (b) the successive LP approximation algorithm in [2] for the problem in (17) which mainly differs from the above approximation heuristic in that the approximation is linear and the approximated problems are not solved iteratively but jointly for all users, and (c) single-user water-filling considering a static background noise including the highest possible crosstalk noise based on the other systems transmitting at PSD mask. A novelty we introduce for the comparison of suboptimal DSM algorithms is that after

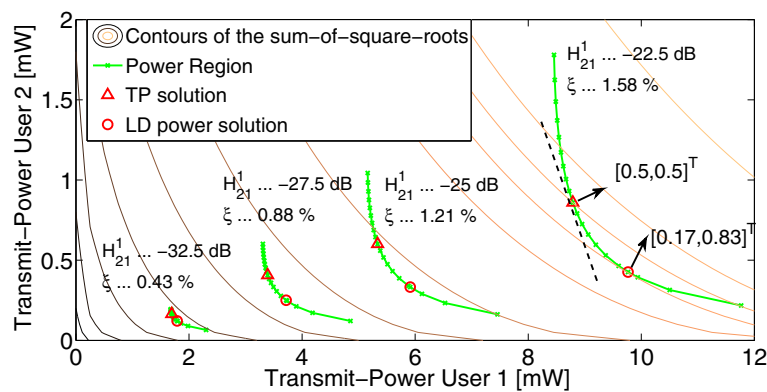


Figure 7 Location of optimization solutions in the power-region. Locations of the solutions to the studied problems in (16) and (17) and the gain ξ by the latter in terms of the LD power consumption.

obtaining the result of a DSM scheme we initialize the respective other DSM algorithm with this result and keep the best solutions in terms of LD power and TP objective, respectively. The purpose of this strategy is to avoid the dependency of the comparison on the initialization which might have been chosen in favor of one of the algorithms^h. The difference to the initialization approach in Section ‘DSM based on successive SINR-approximation and geometric programming’ is that we cross-initialize two heuristics, while in Section ‘DSM based on successive SINR-approximation and geometric programming’ we applied a single heuristic to two different problems.

Based on the insights of the two previous sections we design a network scenario with realistic parameters where we would expect a difference in LD power between the two considered optimization approaches. This is with respect to the selected channel model (a 99% worst-case model [30]), the network topology (a near-far scenario with one CO deployed line and 7 cabinet deployed disturbers), the bandplan (showing strong crosstalk with the CO deployed line, see below), the target-rates (low rates for the CO deployed victim line and high rates for the cabinet lines), and the selected DSL systems (the LD power model for the VDSL cabinet lines has a lower slope than that for the ADSL2+ CO line, cf. Figure 2). More precisely, we consider the near-far downstream scenario shown in Figure 8 with 8 lines deployed in the same cable bundle, where 7 VDSL lines are deployed from a cabinet and one ADSL2+ line is deployed from the CO. We set the parameters of the ADSL2+ line in accordance with the standard in [41] (using the non-overlapping bandplan with ISDN in Annex A) and of the VDSL lines according to [42] with a total SNR gap of $\Gamma = 12.3$ dB in both systemsⁱ. The assigned target-rates are 1, 2, or 3 Mbps and 10, 13, 16, or 19 Mbps for the CO and cabinet deployed lines, respectively, and we investigate all 12 combinations of these target-rates^j.

We observed that due to the heuristic nature of both algorithms the LD power optimization did not always give a better total LD power than the TP optimization (corresponding to a negative gain ξ in (19)). In summary, the gain ξ in (19) was in the studied 12 scenarios between -0.01% and $+0.01\%$. DSM gives a more substantial LD

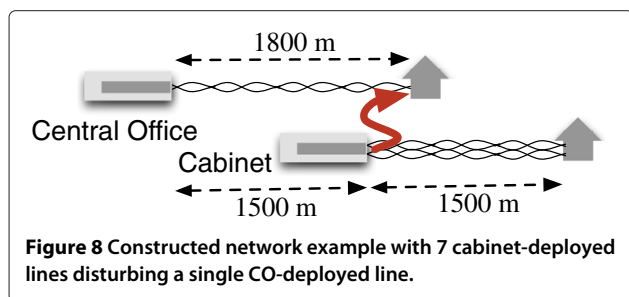
power reduction compared to SSM between 20% and 40%. While this result is no definite answer to whether or not LD power optimization makes a difference compared to TP optimization, it is another indication that in practice the difference may be assumed negligible, which motivates the simplification of the optimization in this direction. However, multi-user DSM bares a substantial potential for energy-reduction compared to SSM, as we shall study further in a larger set of scenarios in the following section.

Average performance evaluation

Differently to the previous section we will next study the possible LD power reduction by TP optimization (DSM) compared to SSM in 300 *randomly* generated network topologies with simulation parameters as specified in Section ‘An experiment in real-sized DSM problems using heuristics’. More precisely, we study two deployment scenarios, where the first one consists of 15 ADSL2+ lines with loop-lengths uniformly sampled between 800 m and 1600 m. The second type of scenarios consists of 15 VDSL cabinet-deployed lines with loop-lengths between 300 and 800 m^k. We compare the TP optimization algorithm in [3] and the SSM algorithm as described in the previous section. Target-rates are set by multiplying the (scenario dependent) maximum achievable per-user rates as achieved by the heuristic in [2] by factors of $\{0.2, 0.4, 0.6, 0, 8\}$. Differently to above, the crosstalk channel model is based on measurements in [43], where we perform a random cable selection for each network sample. Summarizing, the simulation setup does not exaggerate the inter-user crosstalk (e.g., by near-far scenarios or worst-case crosstalk couplings) and therefore provides a realistic evaluation of the energy savings by multi-user DSM compared to SSM.

Next, we present the average LD power consumption results together with 99% confidence intervals according to a student t-test. The average LD power consumption in the ADSL2+ scenarios obtained by the sum-rate maximizing DSM algorithm in [2] leads already to an LD power reduction compared to (spectral mask and sum-power constrained) full-power transmission of 38.70% ($\pm 0.97\%$), which has to be compared to the maximum possible savings by TP reduction (which is obtained by reducing the TP to zero) of 85.69%. Hence, even rate-maximizing DSM can be regarded as an energy saving technology, as already argued in [44]. In the VDSL scenarios the sum-rate maximization leads to an LD power reduction compared to full-power transmission of 9.10% ($\pm 0.46\%$). The maximum possible savings are now only 32.14%, due to the lower sum-power constraint as enforced by the spectral mask, cf. the LD model for VDSL in Figure 2.

The additional savings by energy-efficient (EE) DSM compared to rate-maximizing DSM are shown in Figures 9 and 10. In Figure 9, we see that in the ADSL2+



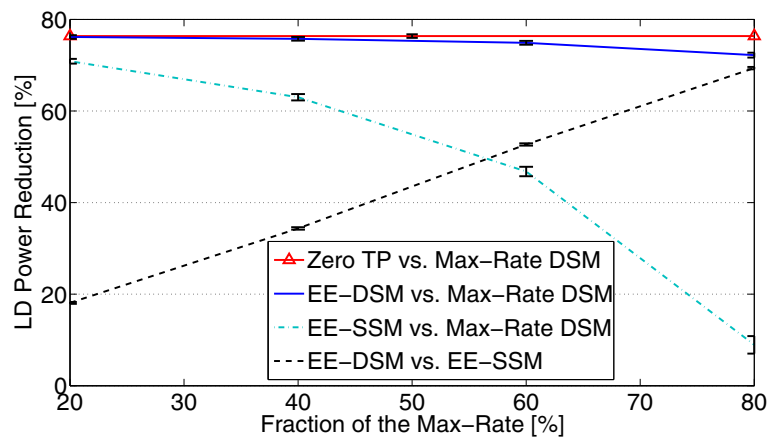


Figure 9 LD power savings achieved by various TP optimization strategies in ADSL2+.

scenarios multi-user DSM gives (on average) more than 70% LD power reduction at 80% of the maximum rates compared to sum-rate maximizing DSM, whereas SSM only results in less than 11% LD power reduction. Hence, DSM gives substantial improvements compared to SSM, most noticeable at higher rates. In the VDSL scenarios the conclusions are qualitatively similar. However, as shown in Figure 10, the LD power reduction at 80% of the maximum rates is now only 23%, whereas SSM results in less than 7% LD power reduction.

Conclusions

We derive novel realistic models of the line-driver (LD) power consumption in class-AB and G LDs as a function of the transmit power (TP) in digital subscriber lines (DSL). These models include non-idealities of the power supply and therefore result in more accurate, higher figures of LD power consumption. Based on the functional shape of the class-AB LD model we exemplarily study its optimization by dynamic spectrum management (DSM).

Multi-user DSM was seen to give substantial energy savings compared to static spectrum management in a large set of DSL scenarios. Furthermore, through an empirical simulation study we were able to identify small DSM problem instances where the TP and the LD power optima provably differ in terms of LD power consumption. However, we were not able to reproduce this difference in simulations for systems of practical size, which suggests that the multi-user DSM problem can be simplified by optimizing TP instead of LD power at negligible performance loss.

Appendix 1

Derivation of the class-AB LD model

In this appendix, we detail the derivation of (2) based on (1), adapted from [26]. The output power in (1) is defined as

$$P_u = \frac{V_{\text{rms,ideal}}^2}{R'_{\text{line}}}, \quad (27)$$

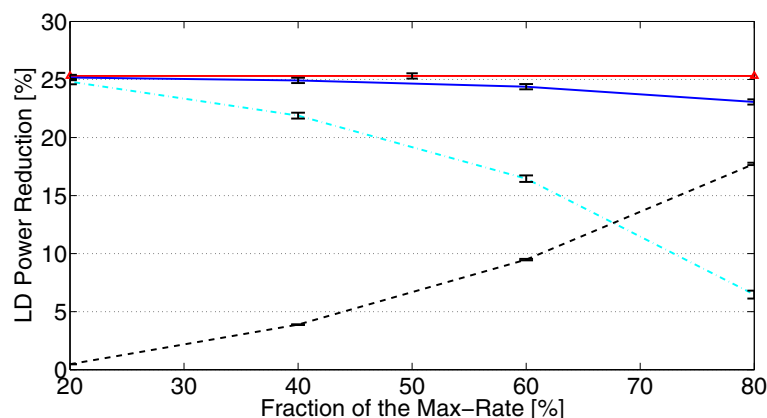


Figure 10 LD power savings achieved by various TP optimization strategies in VDSL.

where $V_{\text{rms,ideal}} = \sqrt{\mathbb{E}\{|V_O|^2\}}$, $V_O \sim \mathcal{N}(0, V_{\text{rms,ideal}}^2)$ is the normal distributed output voltage (cf. Figure 1), $R'_{\text{line}} = R_{\text{line}}/n^2$ is the transformed resistance of the line, and n is the transformer ratio. The average dissipated power P_{diss} can be decomposed into the quiescent power P_Q and the dissipated power associated with the voltage drop in the class-AB design [46], according to

$$P_{\text{diss}} + P_u = P_Q + \mathbb{E} \left\{ (V_s - |V_O|) \frac{|V_O|}{R'_{\text{line}}} \right\} + P_u \quad (28a)$$

$$= P_Q + \frac{V_s}{R'_{\text{line}}} \mathbb{E}\{|V_O|\} \quad (28b)$$

$$= V_s \cdot I_Q + \frac{V_s}{R'_{\text{line}}} \sqrt{\frac{2}{\pi}} V_{\text{rms,ideal}}, \quad (28c)$$

where V_s is the supply voltage and in (28a) we use (27), cf. [26] for details. Equation (2) derives by (1) and using (27) in (28c).

Appendix 2

Model of a class G LD with two supplies

The power consumption of a class-G LD with two supply voltages is given as

$$P_{\text{LD}(G-2S)} = P_{\text{Low},2S} + P_{\text{High},2S} + P_{Q,2S} + P_{\text{Hybrid}}, \quad (29)$$

where $P_{\text{Low},2S}$ and $P_{\text{High},2S}$ are the consumed powers when the supply voltage is V_L and V_H , respectively, $P_{Q,2S} = (V_L(1 - \mu_{2S}(P_u)) + V_H \mu_{2S}(P_u)) \cdot I_Q$ is the quiescent power, and $\mu_{2S}(P_u) \in [0, 1]$ is the fraction of time the high supply voltage is active. Assuming a threshold $V_{\text{th}} = (V_L - V_{\text{drop}})$ for switching between the two supplies, where V_{drop} is the voltage drop in the class-AB design, and that the LD's output voltage V_O is Gaussian distributed [26] with zero mean and variance V_{rms}^2 , we have $\mu_{2S}(P_u) = 2Q(\frac{V_{\text{th}}}{V_{\text{rms}}})$, $Q(\cdot)$ denoting the Q-function. Furthermore, $P_{\text{Low},2S}$ is computable as (see [26] for a similar derivation)

$$P_{\text{Low},2S} = \frac{2V_L}{R'_{\text{line}} \text{TL} \frac{m+1}{m}} \int_0^{V_{\text{th}}} \frac{x}{\sqrt{2\pi} V_{\text{rms}}} e^{-\frac{x^2}{2V_{\text{rms}}^2}} dx \quad (30a)$$

$$= V_L \cdot \sqrt{\frac{2}{\pi}} \frac{P_u}{R'_{\text{line}}} \cdot \left(1 - e^{-\frac{(V_L - V_{\text{drop}})^2}{2P_u R'_{\text{line}} (\text{TL} \frac{m+1}{m})^2}} \right), \quad (30b)$$

where the term $R'_{\text{line}} \text{TL} \frac{m+1}{m}$ in (30a) accounts for the total LD output resistance, and in (30b) we use the definition of V_{rms} in (6). Similarly, the power consumption when the supply with the higher voltage level V_H is active is derived as

$$P_{\text{High},2S} = V_H \cdot \sqrt{\frac{2}{\pi}} \frac{P_u}{R'_{\text{line}}} \cdot e^{-\frac{(V_L - V_{\text{drop}})^2}{2P_u R'_{\text{line}} (\text{TL} \frac{m+1}{m})^2}}. \quad (31)$$

These formulas are equivalent to those shown in [4,26], with the exception of the quiescent power calculation and the consideration of the resistance R'_{line} at the primary transformer side, the voltage drop V_{drop} , the transformer loss TL , and the synthesis factor m in the computation of the voltage-level probabilities. Not included in (29) are the extra power losses due to the necessary DC-DC conversion, cf. the discussion in Section 'Line driver modeling'.

We note that the dynamic power (the sum of (30a) and (31)) can also be written as the sum of the power consumed by a supply *always* working at V_L , and that of a supply delivering $(V_H - V_L)$ during a fraction $\mu_{2S}(P_u)$ of the time, cf. the class-G LD model with charge pump in Section 'Class-G line-driver power model' that is based on this interpretation.

Appendix 3

Proof of Proposition 2

Proof. For $U = 1$ and arbitrary C the objective in (17a) is simply a single non-linear, monotonously increasing function (a square-root) of the user's sum-power, and omitting this function does therefore not change the optimum of the problem in (17) [47], yielding an identical formulation as of the transmit power minimization problem in (16). In the case of $C = 1$ and arbitrary U the target-rates in (16b) uniquely define the minimal per-user transmit powers necessary to support the target-rates [48]. However, as the LD power model in (15) as a function of the per-user transmit sum-power is monotonously increasing, any other power allocation feasible in (17b) than this minimal one would have a higher LD power consumption, and the minimum TP solution for the problem in (16) is therefore also optimal in the LD power minimization problem in (17). \square

Appendix 4

A geometric programming (GP) approach for LD power optimization

GPs consist of posynomial objective and inequality constraints, as well as monomial equality constraints. Posynomial functions are sums $\sum_{k=1}^K f_k(\mathbf{p})$ of monomial functions $f_k(\mathbf{p}) : \mathcal{R}_+^{CU} \rightarrow \mathcal{R}$ of the form $f_k(\mathbf{p}) = c_k \cdot p_1^{\alpha_1^k} \cdot p_2^{\alpha_2^k} \cdot \dots \cdot p_{UC}^{\alpha_{UC}^k}$, where $c_k \geq 0$ and $\alpha_i^k \in \mathcal{R}$, $1 \leq i \leq CU$. We refer to [14] for a more detailed introduction to GPs. Introducing auxiliary variables t_u , $u \in \mathcal{U}$, for the sum-power terms $\sum_{c \in \mathcal{C}} p_c^u$ in (17a) we obtain the equivalent formulation

$$\text{minimize } \sum_{u \in \mathcal{U}} \sqrt{t_u} \quad (32a)$$

$$\text{subject to } t_u^{-1} \cdot \sum_{c \in \mathcal{C}} p_c^u \leq 1, \forall u \in \mathcal{U}, \quad (32b)$$

$$\text{Constraints (16b)-(16e)}. \quad (32c)$$

According to the definitions above, the objective in (32a) is a posynomial function and the auxiliary constraints in (32b) have posynomial form [14]. As noted in [15] the constraints in (16b) can also be written as posynomial constraints when using for instance the SINR approximation [11] $r_c^u(\mathbf{p}_c) \approx \tilde{r}_c^u(\mathbf{p}_c) = \alpha_c^u \log_2(\text{SINR}_c^u(\tilde{\mathbf{p}}_c)) + \beta_c^u, c \in \mathcal{C}, u \in \mathcal{U}$, where SINR_c^u is the SINR in (14) and $\tilde{p}_c^u, c \in \mathcal{C}, u \in \mathcal{U}$, is the approximation point. To see this, one needs to introduce additional variables $\tilde{t}_c^u, c \in \mathcal{C}, u \in \mathcal{U}$, replacing the total noise $(\sum_{i \in \mathcal{U} \setminus u} H_c^{ui} p_c^i + N_c^u)$ user u receives on subcarrier c . The thereby created additional constraints $\tilde{t}_c^u \geq (\sum_{i \in \mathcal{U} \setminus u} H_c^{ui} p_c^i + N_c^u), c \in \mathcal{C}, u \in \mathcal{U}$, are posynomial expressions. Under these additional variables the constraints in (16c) and (16d)-(16e) can be seen to be already given in posynomial and monomial form, respectively. Hence, we have that the problem in (32) can be approximated as a GP which is efficiently and optimally solvable by convex optimization software [49].

Appendix 5

A box-based branch-and-reduce algorithm

Algorithm 1 schematically describes the proposed scheme for global optimization of the DCP problem in (26). The idea behind the method is to first enclose the set defined by the mask-constraints in (26c) by a box, cf. Line 2, and to successively split this set (“branching”) into smaller boxes, cf. Line 4. We observed that box-based branching repeatedly outperforms simplicial branching [50]. We believe this is due to the conservative initial search space in simplicial branching, which is a simplex with corner points $\mathbf{0}, (\sum_{u \in \mathcal{U}, c \in \mathcal{C}} \hat{p}_c^u) \mathbf{e}_u, u \in \mathcal{U}$, where \mathbf{e}_u is the u ’th unit vector. Lower bounds on the objective value in any box are computed by linear programming (LP) after linearly approximating (underestimating) all convex functions $g_u(\mathbf{p})$ and all concave functions $-h_u(\mathbf{p}), u \in \mathcal{U}$, cf. Line 5. The fact that such a linear underestimation of convex and concave functions can easily be found [50] is the key advantage of the DCP formulation in (26). Differently to [50] we propose to apply linear approximations of all convex functions $g_u(\mathbf{p}), u \in \mathcal{U}$, not only on a single point but on various points in the considered box, e.g., in regular intervals between the center point and each corner point. Based on the lower-bounds and the best feasible solution found so far (the “incumbent”) the created boxes are either further split or discarded if the lower-bound lies above the upper bound, cf. Line 8. More precisely, in [37] a transformation of variables into dB-scale was proposed. Similarly we perform the branching (bisection) in dB-scale, which has the advantage that we still consider the full search-space beginning at a power allocation of zero. More precisely, in Line 4, we subdivide a box along its longest edge in dB-scale. In case the value of the minimal element in splitting dimension is zero we use a lower

value based on a fixed ratio to the value of the maximal element in splitting dimension.

Another technique integrated in Algorithm 1 is that of range reduction [51,52]. Briefly speaking, bounds of constraints in the LP used to compute lower bounds can be tightened based on the obtained optimal dual variables associated with these constraints and the current incumbent solution, cf. [51,52] for details. Note that we omitted any local search step for improving the incumbent solution as is typically done in continuous BnB methods [52]. We believe the incumbent initialization in Line 1 by the successive geometric programming described in Appendix 4 is tight enough for the considered applications to make such a local search in the BnB process redundant. We refer to [50] for a detailed description of a basic *simplicial* branch-and-bound algorithm applied to a general DCP problem, and to [51] for an introduction to the range-reduction technique, as well as to [53] for an application of range reduction in a specific DCP problem with DCP functions in the objective only.

Algorithm 1 Box-based Branch-and-Reduce Algorithm

- 1: Initialize the incumbent using a heuristic solution based on successive geometric programming, cf. Section ‘DSM based on successive SINR-approximation and geometric programming’.
- 2: Initialize the first open, currently active box with minimal and maximal corner-points $\mathbf{0} \in \mathcal{R}^{UC}$ and $\hat{\mathbf{p}} \in \mathcal{R}^{UC}$.
- 3: **while** {Any box is open} **do**
- 4: Branching: Generate two new open boxes by splitting the currently active box in half in dB-scale in the dimension of its longest edge.
- 5: Bounding: Compute objective lower bounds for both new boxes using an underestimating LP [50] to the DCP problem in (26) with reduced variable ranges [51].
- 6: Reduction: Try a range-reduction based on the current incumbent solution [51], and repeat the lower-bound LP if a range-reduction was achieved.
- 7: Incumbent Update: Update the incumbent by testing the 2^{CU-1} new corner points created through branching and the LP solutions for feasibility in (26).
- 8: Pruning: Close all boxes with a lower bound above the incumbent solution.
- 9: Selection: Choose the open box with the lowest lower bound as the new active box.

Endnotes

^aThe parameters chosen for ADSL2+ are $R_{\text{line}} = 100\Omega$, $n = 1.25$, $CF = 5.3$, $\hat{P}_u = 19.5\text{dBm}$, $TL = 0.5\text{dB}$, $m = 5$, $I_Q = 5\text{mA}$, $V_{\text{drop}} = 4\text{V}$, and $P_{\text{Hybrid}} = 0$. The parameters

for VDSL deviating from these values are $I_Q = 11.1\text{mA}$ and $\hat{P}_u = 11.5\text{dBm}$.

^bThe selected profiles correspond to downstream ADSL2+ (Annex A) [41] and VDSL2 [45] profiles 8b (Annex A), 17a (Annex B), and 30a. The chosen parameters common to all LD models are $R_{\text{line}} = 100\Omega$, $n = 1.4$ (as in [29]), $\hat{P}_u = 20.5\text{dBm}$ (14.5dBm) for ADSL2+ and VDSL2 profile 8b (VDSL2 profile 17a and 30a), $TL = 0.5\text{dB}$, $m = 5$, $V_{\text{drop}} = 5\text{V}$, and $P_{\text{Hybrid}} = 0$. For the class-AB model we assume $CF = 5.3$. The quiescent currents $I_Q \in 0.95 * \{7.6, 9.8, 12, 18\}\text{mA}$ for the four profiles were selected according to the values suggested in [29] and scaled by a factor of 0.95 that accounts for the diversion of quiescent current to the load [28]. While for the class-AB LD the optimal supply voltage in (3) is assumed, for the class-G LD with two supplies we consider $V_H = 24\text{V}$, and for the LD with charge pumps we set $V_H = 24\text{V} + V_{\text{drop,cp}}$, $I_{Q,\text{classG}} = 0.3\text{mA}$, $L_{\text{classG}} = 0\text{mW}$, and $\rho = 1.5\text{dB}$, where $V_{\text{drop,cp}} = 2\text{V}$ represents an additional voltage drop due to the charging circuitry and a margin necessary due to the permanent discharging of the charge pump capacitors. For both class-G LD types we set $V_L = 12\text{V}$ and assume a threshold for switching between high and low supply of $V_{\text{th}} = V_L - V_{\text{drop}}$. The usage probability $\mu_{\text{cp}}(P_u)$ is obtained through simulations for different values of P_u . The charge pump is assumed to be active for a time-frame of $0.11\mu\text{s}$ (ADSL2+ and VDSL2 8b), $0.04\mu\text{s}$ (VDSL2 17a) or $0.05\mu\text{s}$ (VDSL2 30a) when V_{rms} exceeds V_{th} . Additionally it is assumed to be active for $0.35\mu\text{s}$ and $0.5\mu\text{s}$ before and after this time-frame, which accounts for the charging and discharging of the charge pump capacitors, respectively.

^cThe specific parameters assumed throughout the rest of the article are those mentioned in Section ‘Class-AB line-driver power model’ with the exception of $n = 1.2$, $CF = 5$, and the power limit $\hat{P}_u = 19.9\text{dBm}$ used for ADSL2+ lines.

^dThe remaining relevant parameters are $H_c^{uu} = 1$, $\Gamma = 12.3\text{dB}$, $\Delta = 4.3125 \cdot 10^3 [\text{Hz}]$, $N_c^u = 10^{-140/10} \cdot \Delta [\text{mW}]$, $\hat{p}_c^u = 10^{-40/10} \cdot \Delta [\text{mW}]$, $u \in \mathcal{U}$, $c \in \mathcal{C}$, $\hat{B} = \infty$.

^eThis sequential re-initialization process is stopped in case the best solution found for both problems does not improve for more than three consecutive iterations.

^fBy multiplication with 500 we heuristically scale the transmit sum-power values to that of a system with 1000 subcarriers in order to obtain LD power values through our LD power model which are somewhat comparable to those under more realistic system parameters in the following sections.

^gThe relevant selected parameters are those of Section ‘DSM based on successive SINR-approximation and geometric programming’ with the exception of $R_1 = 41.36[\text{bits/frame}]$, $R_2 = 5.9[\text{bits/frame}]$,

$H_c^{12} = -67.5\text{dB}$ and the initial value $H_c^{21} = -22.5\text{dB}$, $c \in \mathcal{C} = \{1, 2\}$.

^hThe sequential re-initialization process is stopped if no improvement of the best solution found by any of the algorithms was detected for two consecutive iterations. The PSD for the TP optimization and its first approximation was initialized at a low level of -120dBm per subcarrier and user. The trust-region used in the LD power optimization scheme in [2] is set to -70dBm per subcarrier and user after being initialized with the solution of the sequential TP minimization algorithm in [3].

ⁱWe consider the bandplan setting for fiber-to-the-exchange, mask variant B, and un-notched mask M2, which would not be used in practice in this form due to the high ingress noise into ADSL lines but serves our purpose to imitate the insightful scenarios found in Section ‘DSM based on successive SINR-approximation and geometric programming’.

^jThe maximum rate for the VDSL lines in the considered scenario as found by the LD power optimization algorithm [2] is approximately 19.9Mbps .

^kSimulation parameters for both DSL technologies are as specified in Section ‘An experiment in real-sized DSM problems using heuristics’, except that for VDSL we use the bandplan specified in [42] for fiber-to-the-cabinet, mask variant A-M1.

Competing interests

The authors declare that they have no competing interests.

Acknowledgements

This work has been funded by BMVIT/FFG under the program FIT-IT. The Competence Center FTW Forschungszentrum Telekommunikation Wien GmbH was funded within the program COMET—Competence Centers for Excellent Technologies by BMVIT, BMWA, and the City of Vienna. The COMET program was managed by the FFG.

Author details

¹FTW Telecommunications Research Center Vienna, Donau-City-Straße 1, A-1220 Vienna, Austria. ²Lantiq A GmbH, Siemensstraße 4, A-9500 Villach, Austria. ³Centre for Research on Embedded Systems, Halmstad University, Box 823, SE-30118 Halmstad, Sweden.

Received: 16 February 2012 Accepted: 30 August 2012

Published: 25 October 2012

References

1. K Hooghe, M Guenach, in *IEEE Global Communications Conference 2011 (GLOBECOM'11)*. Towards energy-efficient packet processing in access nodes (Houston, Texas, USA, 2011), pp. 1–6
2. M Guenach, C Nuzman, J Maes, M Peeters, in *International Workshop on Green Communications, IEEE GLOBECOM*, vol. 2009. Trading Off Rate and Power Consumption in DSL Systems (Honolulu, Hawaii, 2009), pp. 1–5
3. M Wolkerstorfer, D Statovci, T Nordström, in *IEEE International Conference on Communications Systems 2008 (ICCS'08)*. Dynamic Spectrum Management for Energy-Efficient Transmission in DSL (Guangzhou, China, 2008), pp. 1015–1020
4. M Guenach, C Nuzman, K Hooghe, J Maes, M Peeters, in *International Workshop on Green Communications, IEEE GLOBECOM 2010*. Reduced dimensional power optimization using class AB and G line drivers in DSL (USA, Miami, 2010), pp. 1443–1447

5. M Guenach, C Nuzman, K Hooghe, J Maes, M Peeters, in *On power-efficient usage of line drivers in copper-based access networks*, in *IEEE International Energy Conference and Exhibition (EnergyCon'10)* (Manama, Bahrain, 2010), pp. 131–136
6. P Tsiiaflakis, Y Yi, M Chiang, M Moonen, DSL Green, in *IEEE International Conference on Communications 2009 (ICC'09)*. Energy-Efficient DSM (Dresden, Germany, 2009), pp. 1–5
7. M Guenach, C Nuzman, J Maes, M Peeters, in *IEEE International Conference on Communications Workshops (ICC'09)*. On Power Optimization in DSL Systems (Dresden, Germany, 2009), pp. 1–5
8. M Wolkerstorfer, Energy-efficient resource allocation in multi-carrier digital subscriber lines. PhD thesis. Vienna University of Technology, Vienna, Austria, 2012
9. KB Song, ST Chung, G Ginis, J Cioffi, Dynamic spectrum management for next-generation DSL systems. *IEEE Commun. Mag.* **40**(10), 101–109 (2002)
10. B Johansson, P Soldati, M Johansson, Mathematical decomposition techniques for distributed cross-layer optimization of data networks. *IEEE J. Sel. Areas Commun.* **24**(8), 1535–1547 (2006)
11. J Papandriopoulos, J Evans, S C A L E: A low-complexity distributed protocol for spectrum balancing in multiuser DSL networks. *IEEE Trans. Inf. Theory.* **55**(8), 3711–3724 (2009)
12. P Tsiiaflakis, M Diehl, M Moonen, Distributed spectrum management algorithms for multiuser DSL networks. *IEEE Trans. Signal Process.* **56**(10), 4825–4843 (2008)
13. M Wolkerstorfer, J Jaldén, T Nordström, Column generation for discrete-rate multi-user and multi-carrier power control. *IEEE Trans. Commun.* **60**(9), 2712–2722 (2012). doi:10.1109/TCOMM.2012.070912.110444
14. S Boyd, SJ Kim, L Vandenberghe, A Hassibi, A tutorial on geometric programming. *Optimiz. Eng.* **8**, 67–127 (2007)
15. M Chiang, C Tan, D Palomar, D O'Neill, D Julian, Power control by geometric programming. *IEEE Trans. Wirel. Commun.* **6**(7), 2640–2651 (2007)
16. R Horst, P Pardalos, N Thoai, *Introduction to Global Optimization, Volume 48 of Nonconvex Optimization and its Applications*. (Kluwer Academic Publishers, Dordrecht, 2000), pp. 1–353
17. The Climate Group: SMART 2020, Enabling the low carbon economy in the information age (2008)
18. EC Directorate-General JRC Joint Research Centre, Institute for Energy, Renewable Energy Unit: Code of Conduct on Energy Consumption of Broadband Equipment. *Version 4* (2011)
19. R Bolla, F Davoli, R Bruschi, K Christensen, F Cucchietti, S Singh, The potential impact of green technologies in next-generation wireline networks: Is there room for energy saving optimization. *IEEE Commun. Mag.* **49**(8), 80–86 (2011)
20. T Piessens, M Steyaert, *Design and analysis of high efficiency line drivers for xDSL*. (Kluwer Academic Publishers, Dordrecht, 2004), pp. 1–235
21. B Serneels, M Steyaert, *Design of High Voltage xDSL Line Drivers in Standard CMOS*. (Springer, Dordrecht, 2008), pp. 1–185
22. M Guenach, C Nuzman, J Maes, M Peeters, Y Li, D Van Bruyssel, F Defoort, Power efficient copper access. *Bell Labs Tech J.* **15**(2), 117–129 (2010)
23. M Wolkerstorfer, D Statovci, T Nordström, Energy-Saving by Low-Power Modes in ADSL2. Elsevier Comput. Netws Special Issue on Green Communication Networks. **56**(10), 2468–2480 (2012)
24. I Kamitsos, P Tsiiaflakis, S Ha, M Chiang, in *IEEE Global Communications Conference 2011 (Globecom'11)*. Stable Sleeping in DSL Broadband Access: Feasibility and Tradeoffs (Houston, Texas, USA, 2011), pp. 1–6
25. K Hooghe, M Guenach, in *IEEE Symposium on Communications and Vehicular Technology in the Benelux 2010 (SCVT'10)*. Impact of FTTH architecture on access node energy efficiency (Enschede, The Netherlands, 2010), pp. 1–5
26. J Pierdomenico, S Wurcer, B Day, A 684-mW adaptive supply full-rate ADSL CO driver. *IEEE J. Solid-State Circ.* **37**(12), 1831–1838 (2002)
27. S Wurcer, Carefully evaluate your ADSL line-driver efficiency. *Commun. Syst. Design.* **2003**, 21–23 (2003)
28. R Stephens, Active output impedance for ADSL line drivers. *Texas Instrum. Analog Appl. J.* **Q4**, 24–31 (2002)
29. TI, H Gated-Class, Dual-Port VDSL2 Line Driver. Tech. Rep. THS 6226, Texas Instruments (2011)
30. P Golden, H Dedieu, K Jacobsen, *Fundamentals of DSL Technology*. (Auerbach Publications, Boca Raton, 2006), pp. 1–472
31. R Cendrillon, F Liming, J Chou, G Long, C Hung, D Wei, in *IEEE Global Communications Conference 2008 (GLOBECOM'08)*. D S M from theory to practice (New Orleans, LA, USA, 2008), pp. 1–4
32. E Medeiros, N Lindqvist, M Monteiro, H Abraham, F Lindqvist, B Dortschy, A Klautau, in *European Signal Processing Conference 2009 (Eusipco'09)*. DSM performance on practical DSL systems based on estimated crosstalk channel information (Glasgow, Scotland, 2009), pp. 2092–2096
33. R Cendrillon, W Yu, M Moonen, J Verlinden, T Bostoen, Optimal multiuser spectrum balancing for digital subscriber lines. *IEEE Trans. Commun.* **54**(5), 922–933 (2006)
34. P Tsiiaflakis, Y Yi, M Chiang, M Moonen, Fair greening for DSL broadband access. *ACM SIGMETRICS Perf. Eval. Rev.* **37**(4), 74–78 (2010)
35. M Wolkerstorfer, T Nordström, *Coverage optimization in DSL networks by low-complexity discrete spectrum balancing*. (Houston, Texas, USA, 2011), pp. 1–6
36. J Brehmer, W Utschick, Nonconcave utility maximisation in the MIMO broadcast channel. *EURASIP J. Adv. Signal Process.*, 1–13 (2009). Article ID 645041
37. Y Xu, T Le-Ngoc, S Panigrahi, Global concave minimization for optimal spectrum balancing in multi-user DSL networks. *IEEE Trans. Signal Process.* **56**(7), 2875–2885 (2008)
38. K Eriksson, S Shi, N Vucic, M Schubert, E Larsson, in *IEEE Global Telecommunications Conference (GLOBECOM'10)*. Globally optimal resource allocation for achieving maximum weighted sum rate (USA, Miami, 2010), pp. 1–6
39. M Charafeddine, A Paulraj, in *Conference on Information Sciences and Systems (CISS'07)*. Sequential geometric programming for 2x2 interference channel power control (Baltimore, MD, USA, 2007), pp. 185–189
40. R Horst, P Pardalos, *Handbook of Global Optimization, Volume 2 of Nonconvex Optimization and its Applications*. (Kluwer Academic Publishers, Dordrecht, 1995), pp. 1–575
41. ITU-T, Asymmetric digital subscriber line (ADSL) transceivers - Extended bandwidth ADSL2 (ADSL2+). *G.992.5* (2005)
42. ETSI, Transmission and Multiplexing (TM); Access transmission systems on metallic access cables; Very high speed Digital Subscriber Line (VDSL); Part 1 Functional requirements. *TM6 TS 101 270-1, Version 1.3.1* (2003)
43. D Statovci, T Nordström, in *European Signal Processing Conference 2004 (Eusipco'04)*. Adaptive resource allocation in multiuser FDD-DMT systems (Vienna, Austria, 2004), pp. 1213–1216
44. J Cioffi, H Zou, A Chowdhery, W Lee, S Jagannathan, in *IEEE Global Telecommunications Conference 2008 (GLOBECOM)*. Greener copper with dynamic spectrum management (New Orleans, LA, USA, 2008), pp. 1–5
45. ITU-T, Very high speed digital subscriber line transceivers 2 (VDSL2). *G.993.2* (2006)
46. R van der Zee, High Efficiency Audio Power Amplifiers Design and practical use. *PhD thesis*, Twente University (1999)
47. S Boyd, L Vandenberghe, *Convex Optimization*. (Cambridge University Press, Cambridge, 2004), pp. 1–716
48. R Yates, A framework for uplink power control in cellular radio systems. *IEEE J. Sel. Areas Commun.* **13**(7), 1341–1347 (1995)
49. ApS Mosek, *The MOSEK optimization toolbox for MATLAB manual*. Version 6.0 (Rev 106), Copenhagen, Denmark, (2011)
50. R Horst, N Thoai, DC Programming: Overview. *J. Optimiz. Theory Appl.* **103**, 1–43 (1999)
51. H Ryoo, N Sahinidis, A branch-and-reduce approach to global optimization. *J. Global Optimiz.* **8**(2), 107–138 (1996)
52. N Sahinidis, *BARON - Branch and Reduce Optimization Navigator*. Version 4.0, University of Illinois at Urbana-Champaign (2000)
53. R Cambini, F Salvi, A branch and reduce approach for solving a class of low rank d.c. programs. *J. Comput. Appl. Math.* **233**, 492–501 (2009)

doi:10.1186/1687-6180-2012-226

Cite this article as: Wolkerstorfer et al.: Modeling and optimization of the line-driver power consumption in xDSL systems. *EURASIP Journal on Advances in Signal Processing* 2012 **2012**:226.